



Performance of multi-stage fractured horizontal wells with stimulated reservoir volume in tight gas reservoirs considering anomalous diffusion

Junjie Ren^{1,2} · Ping Guo¹ · Song Peng³ · Zhongliang Ma⁴

Received: 14 January 2018 / Accepted: 8 November 2018 / Published online: 20 November 2018
© Springer-Verlag GmbH Germany, part of Springer Nature 2018

Abstract

Horizontal well combined with volume fracturing technology has been extensively employed in the development of tight gas reservoirs. The disordered distribution of the induced and natural fractures in the reservoirs leads to the existence of the anomalous diffusion, so the conventional Darcy law has some limitations in describing the fluid flow under this circumstance. This paper introduces the fractional Darcy law to take into account the effect of the anomalous diffusion and then extends the conventional model of the multi-stage fractured horizontal (MSFH) well with the presence of the stimulated reservoir volume (SRV). The generated point source model for dual-porosity composite system includes the fractional calculus and its solution in Laplace space is derived. The superposition principle and the numerical discrete method are applied to obtain the solution for the MSFH well with SRV. Stehfest inversion method is used to transform the pseudo-pressure and production rate from Laplace space to real space. Type curves for pseudo-pressure and production rate are presented and analyzed. The influence of the relevant parameters on pseudo-pressure behavior and production rate decline is discussed in detail. The proposed model enriches the flow models of the MSFH well with SRV and can be used to more accurately interpret and forecast the transient pressure and transient rate.

Keywords Anomalous diffusion · Fractional Darcy law · Multi-stage fractured horizontal well · Stimulated reservoir volume · Performance analysis

List of symbols

c_t	Total compressibility, /Pa	k_β	Permeability with the effect of the anomalous diffusion, see Eq. (1), $m^2/s^{\beta-1}$
c_ρ	Gas compressibility, /Pa	L	Half-length of horizontal well, m
c_ϕ	Rock compressibility, /Pa	L_{fLi}, L_{fRi}	Length of left/right wing in the i th hydraulic fracture, m
h	Reservoir thickness, m	m	Hydraulic-fracture number
k	Permeability without the effect of the anomalous diffusion, see Eq. (4), m^2	M	Molar mass of gas, kg/mol
		M_{12}	Mobility ratio between SRV and URV regions
		p	Reservoir pressure, Pa
		p_i	Initial reservoir pressure, Pa
		p_{sc}	Pressure at standard condition, Pa
		p_w	Bottomhole pressure, Pa
		q	Flow rate of point source, m^3/s
		q_f	Flow-rate density of hydraulic fracture, m^2/s
		Q_{sc}	Well-production rate at standard condition, m^3/s
		r	Radial distance, $r = \sqrt{x^2 + y^2}$, m
		r_f	SRV radius, m
		R	Universal gas constant, $8.314J/(K mol)$

✉ Junjie Ren
renjunjie1900@126.com

¹ State Key Laboratory of Oil and Gas Reservoir Geology and Exploitation, Southwest Petroleum University, Chengdu 610500, Sichuan, China

² School of Sciences, Southwest Petroleum University, Chengdu 610500, Sichuan, China

³ Research Institute of Exploration and Development of Zhongyuan Oilfield, SINOPEC, Puyang 457001, Henan, China

⁴ No.1 Oil Production Plant of Qinghai Oilfield Company, PetroChina, Haixi State 816499, Qinghai, China

s	Laplace transform variable
t	Time, s
T	Reservoir temperature, K
T_{sc}	Temperature at standard condition, K
W_{12}	Storability ratio between SRV and URV regions
x, y	x - and y -coordinates, m
y_{wDi}	Dimensionless y -coordinate of the i th hydraulic fracture
Z	Z -factor of gas
α	Shape factor, /m ²
β	Anomalous diffusion exponent
$\Delta L_{iLDi}, \Delta L_{iRD}$	Dimensionless length of discrete segment of the left/right wing in the i th hydraulic fracture
$\Delta\psi_w$	Bottomhole pseudo-pressure difference, $\Delta\psi_w = \psi_i - \psi_w, \text{Pa}^2/(\text{Pa s})$
λ	Interporosity flow coefficient
μ	Gas viscosity, Pa s
ρ	Gas density, kg/m ³
v	Gas velocity, m/s
ψ	Reservoir pseudo-pressure, Pa ² /(Pa s)
ψ_i	Initial reservoir pseudo-pressure, Pa ² /(Pa s)
ψ_w	Bottomhole pseudo-pressure, Pa ² /(Pa s)
ϕ	Porosity
ω_{1f}	Fracture-system storability coefficient in SRV
ω_{2f}	Fracture-system storability coefficient in URV
Subscripts	
D	Dimensionless
f	Fracture system
i, j	The j th discrete segment in the i th hydraulic fracture
m	Matrix system
1	SRV region
2	URV region
Superscripts	
–	Laplace space

Introduction

In the past decades, many tight gas reservoirs with ultra-low permeability have been discovered and developed around the world. It has been proved in practice that horizontal well combined with volume fracturing technology is considered as an effective way to develop tight gas reservoirs. Massive hydraulic fracturing creates several main hydraulic fractures as well as an induced fracture network around them (Clarkson 2013). The fracture network is usually called stimulated

reservoir volume (SRV), in which the reservoir properties are very different from those of unstimulated reservoir volume (URV) (Mayerhofer et al. 2010).

Compared with the conventional models of the multi-stage fractured horizontal (MSFH) wells without SRV (Wang and Yi 2018; Ren and Guo 2018a, b), the models of the MSFH wells with SRV are much more complex. Recently, various models have been established to study the performance of the MSFH wells with SRV. Ozkan et al. (2011) used the tri-linear flow model to investigate the transient pressure for the MSFH well with SRV. Some scholars improved the flow model proposed by Ozkan et al. (2011) to incorporate multiple mechanisms (Apaydin et al. 2012; Tian et al. 2014) or to consider more linear-flow regions (Stalgorova and Mattar 2012; Yuan et al. 2015). However, the tri-linear flow model and its improved versions cannot describe some flow characteristics of the MSFH well with SRV (e.g., the radial flow and the hydraulic-fracture interference). Zhao et al. (2014) employed the point-source function method to establish the flow model of the MSFH well considering the impact of the SRV and studied the performance of the MSFH well. Zeng et al. (2015) and Xu et al. (2015a) established flow models of the MSFH well with SRV in a shale gas reservoir including multiple mechanisms such as desorption, diffusive flow and stress sensitivity. Xu et al. (2015b) proposed a dual-porosity composite model of the MSFH well with elliptical SRV in tight reservoirs. Wei et al. (2016) presented a numerical composite model of the MSFH well with elliptical SRV region for each hydraulic fracture and studied the characteristic of the Blasingame's type curves of the MSFH well. Guo et al. (2016) extended the previous model (Xu et al. 2015a) to establish a more comprehensive model of an MSFH well in a shale gas reservoir, which can consider the impact of the presence of the SRV, fracture conductivity and multiple transport mechanisms. Ren and Guo (2017) proposed a composite model of the MSFH well with SRV taking into account the impact of the quadratic gradient term. Chen et al. (2018) established an arbitrary composite model of the MSFH well with SRV based on boundary element method and investigated the effect of the shape and size of the SRV on the pressure response and production performance. However, as far as we know, previous models for the MSFH well with SRV are established by incorporating the classical Darcy law, which cannot capture the anomalous diffusion in fractured reservoirs (Raghavan and Chen 2013a, 2015) and may lead to errors in the prediction of the transient pressure and transient rate for the MSFH well with SRV. It has been found that the fractional Darcy law, which is the generalized form of the classical Darcy law, can be used to describe the anomalous diffusion and is more suitable for the fractured

reservoirs. In recent years, some seepage models for various wells in fractured reservoirs have been established by incorporating the fractional Darcy law into the governing equations, such as vertical wells (Raghavan 2012a; Razminia et al. 2014), fractured vertical wells (Raghavan 2012b; Raghavan and Chen 2013a), horizontal wells (Raghavan and Chen 2015), MSFH wells (Raghavan and Chen 2013b, 2017; Ren and Guo 2015), and so on. However, there is no work to study the model of the MSFH well with SRV by incorporating the fractional Darcy law. Therefore, the existing models of the MSFH well with SRV have some limitations in interpreting and forecasting the transient pressure and transient rate.

In this paper, we introduce the fractional Darcy law to develop the model of the MSFH well with SRV in tight gas reservoirs. The proposed model can take into account the effect of the anomalous diffusion in fractured rocks, and thus it has a wider application compared to the previous models.

Physical model

The physical model is shown in Fig. 1 and based on the assumptions as follows:

1. The tight gas formation is viewed as a composite system including the inner and outer regions. Both the regions are dual-porosity medium systems with different physical properties of reservoir rocks. The inner and outer regions denote the SRV and URV, respectively.
2. Gas flow in the porous medium obeys the fractional Darcy law, and the interporosity flow between the matrix and fracture systems follows the pseudo-steady model proposed by Warren and Root (1963).
3. An MSFH well is located in the SRV region and produces at a constant rate or a constant bottomhole pres-

sure. Each infinite-conductivity hydraulic fracture perpendicularly intersects with the horizontal wellbore and completely penetrates the reservoir.

Mathematical model

Point source model

Owing to the disordered distribution of natural and induced hydraulic fractures in the tight gas formation, gas flow in the porous medium usually obeys the fractional Darcy law (Raghavan and Chen 2015), which can be written in radial cylindrical coordinate as follows:

$$v(r, t) = -\frac{k_{\beta}}{\mu} \frac{\partial^{1-\beta}}{\partial t^{1-\beta}} \frac{\partial p(r, t)}{\partial r}, \tag{1}$$

where β is anomalous diffusion exponent in the range of $\beta \leq 1$, the definition of the fractional derivative $\partial^{\beta} f(t) / \partial t^{\beta}$ can refer to the literature (Caputo 1967; Xu and Meng 2016; Zuo et al. 2017), which is defined as

$$\frac{\partial^{\beta} f(t)}{\partial t^{\beta}} = \frac{1}{\Gamma(1-\beta)} \int_0^t (t-t')^{-\beta} \frac{\partial f(t')}{\partial t'} dt', \tag{2}$$

where $\Gamma(x)$ is the Gamma function defined by

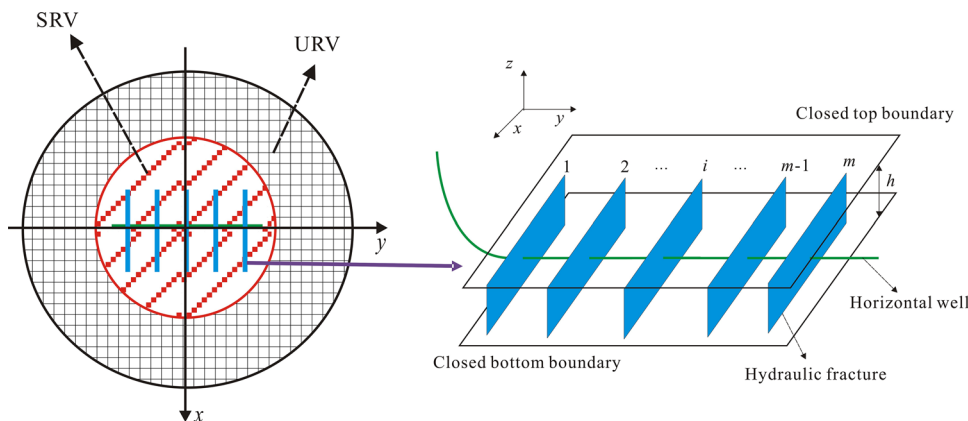
$$\Gamma(x) = \int_0^{\infty} e^{-z} z^{x-1} dz. \tag{3}$$

The expressions with fractional derivative such as Eq. (1) lead to fractional differential equations which have been widely applied in various fields (Zhang et al. 2014, 2017; Feng and Meng 2017; Obembe et al. 2017; Zhang 2017; Li and Wang 2018; Shen et al. 2018).

It is noted that when β is set as one, Eq. (1) becomes the conventional Darcy law:

$$v(r, t) = -\frac{k}{\mu} \frac{\partial p(r, t)}{\partial r}. \tag{4}$$

Fig. 1 Schematic of an MSFH well in a composite system



Compared with the conventional Darcy law, the fractional Darcy law has a much wider field of application and is more suitable for unconventional reservoirs, especially for fractured reservoirs with complex fracture network.

In the following, the point source model in the composite system will be established by introducing the fractional Darcy law.

For inner region (i.e., SRV region) ($0 \leq r \leq r_f$).

On the basis of the mass-conservation law, the continuity equation for the fracture system can be given as

$$\frac{1}{r} \frac{\partial(r\rho_{1f}v_{1f})}{\partial r} + \frac{\partial(\rho_{1f}\phi_{1f})}{\partial t} - q_{1m} = 0. \tag{5}$$

According to the assumption of the pseudo-steady flow (Warren and Root 1963), the continuity equation for the matrix system can be expressed by

$$\frac{\partial(\rho_{1m}\phi_{1m})}{\partial t} + q_{1m} = 0, \tag{6}$$

where q_{1m} in Eqs. (5) and (6) is the matrix-fracture interporosity flow rate, which is given as Warren and Root (1963)

$$q_{1m} = \frac{\alpha_1 k_{1m}}{\mu} (\rho_{1m} p_{1m} - \rho_{1f} p_{1f}). \tag{7}$$

The fractional Darcy law for the SRV region is

$$v_{1f} = -\frac{k_{1\beta}}{\mu} \frac{\partial^{1-\beta_1}}{\partial t^{1-\beta_1}} \frac{\partial p_{1f}}{\partial r}. \tag{8}$$

The real-gas state equations for the matrix and fracture systems in the SRV region are, respectively, written as

$$\rho_{1m} = \frac{p_{1m} M}{ZRT}, \tag{9}$$

$$\rho_{1f} = \frac{p_{1f} M}{ZRT}. \tag{10}$$

The gas compressibility and rock compressibility in the SRV region are, respectively, given as

$$c_{\phi_{1j}} = \frac{1}{\phi_{1j}} \frac{\partial \phi_{1j}}{\partial p_{1j}}, (j = m, f), \tag{11}$$

$$c_{\rho_{1j}} = \frac{1}{\rho_{1j}} \frac{\partial \rho_{1j}}{\partial p_{1j}}, (j = m, f). \tag{12}$$

Substituting Eqs. (8)–(12) into Eqs. (5)–(7), respectively, yields that

$$\frac{\partial^{1-\beta_1}}{\partial t^{1-\beta_1}} \left[\frac{1}{r} \frac{\partial}{\partial r} \left(r \frac{k_{1\beta}}{\mu} \frac{p_{1f} M}{ZRT} \frac{\partial p_{1f}}{\partial r} \right) \right] = \frac{\phi_{1f} c_{11f} p_{1f} M}{ZRT} \frac{\partial p_{1f}}{\partial t} - q_{1m}, \tag{13}$$

$$\frac{\phi_{1m} c_{11m} p_{1m} M}{ZRT} \frac{\partial p_{1m}}{\partial t} + q_{1m} = 0, \tag{14}$$

$$q_{1m} = \frac{\alpha_1 k_{1m} M}{\mu ZRT} (p_{1m}^2 - p_{1f}^2), \tag{15}$$

where $c_{11f} = c_{\rho_{1f}} + c_{\phi_{1f}}$ and $c_{11m} = c_{\rho_{1m}} + c_{\phi_{1m}}$.

For outer region (i.e., URV region) ($r_f \leq r < \infty$).

In the same way, the continuity equation for the fracture system can be expressed as

$$\frac{1}{r} \frac{\partial(r\rho_{2f}v_{2f})}{\partial r} + \frac{\partial(\rho_{2f}\phi_{2f})}{\partial t} - q_{2m} = 0. \tag{16}$$

The continuity equation for the matrix system is

$$\frac{\partial(\rho_{2m}\phi_{2m})}{\partial t} + q_{2m} = 0, \tag{17}$$

and the matrix–fracture interporosity flow rate is given as (Warren and Root 1963)

$$q_{2m} = \frac{\alpha_2 k_{2m}}{\mu} (\rho_{2m} p_{2m} - \rho_{2f} p_{2f}). \tag{18}$$

The fractional Darcy law for the URV region is

$$v_{2f} = -\frac{k_{2\beta}}{\mu} \frac{\partial^{1-\beta_2}}{\partial t^{1-\beta_2}} \frac{\partial p_{2f}}{\partial r}. \tag{19}$$

The real-gas state equations for the URV region are written as

$$\rho_{2m} = \frac{p_{2m} M}{ZRT}, \tag{20}$$

$$\rho_{2f} = \frac{p_{2f} M}{ZRT}. \tag{21}$$

The gas compressibility and rock compressibility in the URV region are, respectively, given as

$$c_{\phi_{2j}} = \frac{1}{\phi_{2j}} \frac{\partial \phi_{2j}}{\partial p_{2j}}, (j = m, f), \tag{22}$$

$$c_{\rho_{2j}} = \frac{1}{\rho_{2j}} \frac{\partial \rho_{2j}}{\partial p_{2j}}, (j = m, f). \tag{23}$$

Substituting Eqs. (19)–(23) into Eqs. (16)–(18), one can obtain that

$$\frac{\partial^{1-\beta_2}}{\partial t^{1-\beta_2}} \left[\frac{1}{r} \frac{\partial}{\partial r} \left(r \frac{k_{2\beta}}{\mu} \frac{p_{2f} M}{ZRT} \frac{\partial p_{2f}}{\partial r} \right) \right] = \frac{\phi_{2f} c_{12f} p_{2f} M}{ZRT} \frac{\partial p_{2f}}{\partial t} - q_{2m}, \tag{24}$$

$$\frac{\phi_{2m} c_{12m} p_{2m} M}{ZRT} \frac{\partial p_{2m}}{\partial t} + q_{2m} = 0, \tag{25}$$

$$q_{2m} = \frac{\alpha_2 k_{2m} M}{\mu ZRT} (p_{2m}^2 - p_{2f}^2), \tag{26}$$

where $c_{12f} = c_{\rho 2f} + c_{\phi 2f}$ and $c_{12m} = c_{\rho 2m} + c_{\phi 2m}$.
Introducing the pseudo-pressure

$$\psi = \int_0^p \frac{2p}{\mu Z} dp, \tag{27}$$

and then Eqs. (13)–(15) and (24)–(26) can be rewritten as

$$\frac{\partial^{1-\beta_1}}{\partial t^{1-\beta_1}} \left[\frac{1}{r} \frac{\partial}{\partial r} \left(r k_{1\beta} \frac{\partial \psi_{1f}}{\partial r} \right) \right] = \phi_{1f} c_{11f} \mu \frac{\partial \psi_{1f}}{\partial t} - \alpha_1 k_{1m} (\psi_{1m} - \psi_{1f}), \quad (0 \leq r \leq r_f), \tag{28}$$

$$\phi_{1m} c_{11m} \mu \frac{\partial \psi_{1m}}{\partial t} + \alpha_1 k_{1m} (\psi_{1m} - \psi_{1f}) = 0, \quad (0 \leq r \leq r_f), \tag{29}$$

$$\frac{\partial^{1-\beta_2}}{\partial t^{1-\beta_2}} \left[\frac{1}{r} \frac{\partial}{\partial r} \left(r k_{2\beta} \frac{\partial \psi_{2f}}{\partial r} \right) \right] = \phi_{2f} c_{12f} \mu \frac{\partial \psi_{2f}}{\partial t} - \alpha_2 k_{2m} (\psi_{2m} - \psi_{2f}), \quad (r_f \leq r < \infty), \tag{30}$$

$$\phi_{2m} c_{12m} \mu \frac{\partial \psi_{2m}}{\partial t} + \alpha_2 k_{2m} (\psi_{2m} - \psi_{2f}) = 0, \quad (r_f \leq r < \infty). \tag{31}$$

The point source is assumed to be placed in the coordinate origin and to produce at a constant rate, so the inner boundary condition can be written as

$$\lim_{r \rightarrow 0} \frac{\partial^{1-\beta_1}}{\partial t^{1-\beta_1}} \left(r \frac{\partial \psi_{1f}}{\partial r} \right) = \frac{p_{sc} q(r=0, t) T}{\pi k_{1\beta} h T_{sc}}. \tag{32}$$

The outer boundary condition is

$$\psi_{2f}(r \rightarrow \infty, t) = \psi_i. \tag{33}$$

The pseudo-pressure and gas velocity should be continuity at the interface between the SRV and URV regions, and thus interface boundary conditions are given as

$$\psi_{1f}(r = r_f, t) = \psi_{2f}(r = r_f, t), \tag{34}$$

$$\frac{\partial^{1-\beta_1}}{\partial t^{1-\beta_1}} \left(k_{1\beta} \frac{\partial \psi_{1f}}{\partial r} \right) \Big|_{r=r_f} = \frac{\partial^{1-\beta_2}}{\partial t^{1-\beta_2}} \left(k_{2\beta} \frac{\partial \psi_{2f}}{\partial r} \right) \Big|_{r=r_f}. \tag{35}$$

With the assumption of the uniform pressure distribution at initial time, the initial condition is expressed as

$$\psi_{1f}(r, t = 0) = \psi_{2f}(r, t = 0) = \psi_{1m}(r, t = 0) = \psi_{2m}(r, t = 0) = \psi_i. \tag{36}$$

Introducing the dimensionless variables which are listed in Table 1, Eqs. (28)–(36) are, respectively, rewritten as

$$\frac{\partial^{1-\beta_1}}{\partial t_D^{1-\beta_1}} \left[\frac{1}{r_D} \frac{\partial}{\partial r_D} \left(r_D \frac{\partial \psi_{1fD}}{\partial r_D} \right) \right] = \omega_{1f} \frac{\partial \psi_{1fD}}{\partial t_D} + \lambda_1 (\psi_{1fD} - \psi_{1mD}), \quad (0 \leq r_D \leq r_{fD}), \tag{37}$$

$$(1 - \omega_{1f}) \frac{\partial \psi_{1mD}}{\partial t_D} - \lambda_1 (\psi_{1fD} - \psi_{1mD}) = 0, \quad (0 \leq r_D \leq r_{fD}), \tag{38}$$

Table 1 Definition of dimensionless variables

Dimensionless pseudo-pressure	$\psi_D = \frac{\pi k_{1\beta} h T_{sc}}{Q_{sc} p_{sc} T} \left[\frac{k_{1\beta}}{(\phi_{1f} c_{11f} + \phi_{1m} c_{11m}) \mu L^2} \right]^{\frac{1-\beta_1}{\beta_1}} (\psi_i - \psi)$
Dimensionless time	$t_D = \left[\frac{k_{1\beta}}{(\phi_{1f} c_{11f} + \phi_{1m} c_{11m}) \mu L^2} \right]^{\frac{1}{\beta_1}} t$
Dimensionless distance	$r_D = \frac{r}{L}, r_{fD} = \frac{r_f}{L}, x_D = \frac{x}{L}, y_D = \frac{y}{L}, x_{wD} = \frac{x_{wi}}{L}, y_{wD} = \frac{y_{wi}}{L}, L_{fD} = \frac{L_{fi}}{L}, L_{fRD} = \frac{L_{fRi}}{L}$
Fracture-system storability coefficient in SRV	$\omega_{1f} = \frac{\phi_{1f} c_{11f}}{\phi_{1f} c_{11f} + \phi_{1m} c_{11m}}$
Fracture-system storability coefficient in URV	$\omega_{2f} = \frac{\phi_{2f} c_{12f}}{\phi_{2f} c_{12f} + \phi_{2m} c_{12m}}$
Mobility ratio between SRV and URV regions	$M_{12} = \frac{k_{1\beta} / \mu}{k_{2\beta} / \mu}$
Storability ratio between SRV and URV regions	$W_{12} = \frac{\phi_{1f} c_{11f} + \phi_{1m} c_{11m}}{\phi_{2f} c_{12f} + \phi_{2m} c_{12m}}$
Interporosity flow coefficient in SRV	$\lambda_1 = \alpha_1 \frac{k_{1m}}{k_{1\beta}} L^2 \left[\frac{k_{1\beta}}{(\phi_{1f} c_{11f} + \phi_{1m} c_{11m}) \mu L^2} \right]^{\frac{\beta_1-1}{\beta_1}}$
Interporosity flow coefficient in URV	$\lambda_2 = \alpha_2 \frac{k_{2m}}{k_{2\beta}} L^2 \left[\frac{k_{1\beta}}{(\phi_{1f} c_{11f} + \phi_{1m} c_{11m}) \mu L^2} \right]^{\frac{\beta_1-1}{\beta_1}}$
Dimensionless point-source flow rate	$q_D(r_D, t_D) = \frac{q(r, t)}{Q_{sc}}$
Dimensionless flow-rate density of hydraulic fracture	$q_{fD}(x_D, y_D, t_D) = \frac{q_f(x, y, t) L}{Q_{sc}}$
Dimensionless well production rate	$Q_D = \frac{Q_{sc} p_{sc} T}{\pi k_{1\beta} h T_{sc} (\psi_i - \psi_w)} \left[\frac{k_{1\beta}}{(\phi_{1f} c_{11f} + \phi_{1m} c_{11m}) \mu L^2} \right]^{\frac{\beta_1-1}{\beta_1}}$

$$\frac{\partial^{1-\beta_2}}{\partial t_D^{1-\beta_2}} \left[\frac{g_{12}}{r_D} \frac{\partial}{\partial r_D} \left(r_D \frac{\partial \psi_{2fD}}{\partial r_D} \right) \right] = \frac{M_{12} \omega_{2f}}{W_{12}} \frac{\partial \psi_{2fD}}{\partial t_D} + \lambda_2 (\psi_{2fD} - \psi_{2mD}), \quad (r_{fD} \leq r_D < \infty), \tag{39}$$

$$\frac{M_{12}(1 - \omega_{2f})}{W_{12}} \frac{\partial \psi_{2mD}}{\partial t_D} - \lambda_2 (\psi_{2fD} - \psi_{2mD}) = 0, \quad (r_{fD} \leq r_D < \infty), \tag{40}$$

$$\lim_{r_D \rightarrow 0} \frac{\partial^{1-\beta_1}}{\partial t_D^{1-\beta_1}} \left(r_D \frac{\partial \psi_{1fD}}{\partial r_D} \right) = -q_D (r_D = 0, t_D), \tag{41}$$

$$\psi_{2fD}(r_D \rightarrow \infty, t_D) = 0, \tag{42}$$

$$\psi_{1fD}(r_D = r_{fD}, t_D) = \psi_{2fD}(r_D = r_{fD}, t_D), \tag{43}$$

$$\left. \frac{\partial^{1-\beta_1}}{\partial t_D^{1-\beta_1}} \frac{\partial \psi_{1fD}}{\partial r_D} \right|_{r_D=r_{fD}} = \frac{g_{12}}{M_{12}} \left. \frac{\partial^{1-\beta_2}}{\partial t_D^{1-\beta_2}} \frac{\partial \psi_{2fD}}{\partial r_D} \right|_{r_D=r_{fD}}, \tag{44}$$

$$\psi_{1fD}(r_D, t_D = 0) = \psi_{2fD}(r_D, t_D = 0) = \psi_{1mD}(r_D, t_D = 0) = \psi_{2mD}(r_D, t_D = 0) = 0, \tag{45}$$

where

$$g_{12} = \left[\frac{k_{1\beta}}{(\phi_{1f} c_{11f} + \phi_{1m} c_{11m}) \mu L^2} \right]^{\frac{\beta_1 - \beta_2}{\beta_1}}. \tag{46}$$

The point source model in the composite system consists of Eqs. (37)–(46), which can be used to take into account the effect of the anomalous diffusion in fractured reservoirs with complex fracture network. When $\beta_1 = 1$ and $\beta_2 = 1$, the proposed point source model becomes the conventional one proposed by Zhao et al. (2014). Obviously, Eqs. (37)–(46) are fractional differential equations. Recently, the theories and solving methods for fractional differential equations have been investigated by many scholars (Guo 2010; Jiang et al. 2013; Zhu et al. 2016; Hao et al. 2017). Laplace transform is a widely used integral transform in mathematics and engineering that transforms a function of time into a function of complex frequency. Laplace transform from the time domain (i.e., the real space) to the frequency domain (i.e., the Laplace space) can transform differential equations into algebraic equations, and thus Laplace transform has been widely used to solve differential equations (Wang and Yi 2017; Wang et al. 2017; Ren and Guo 2018c).

Laplace transform will be employed to solve the above model and it is defined as follows:

$$\bar{f}(s) = \int_0^\infty f(t_D) e^{-st_D} dt_D, \tag{47}$$

where f is an arbitrary variable in real space. According to the above definition, the Laplace transform of the fractional derivative $\partial^\beta f(t_D) / \partial t_D^\beta$ is given as (Caputo 1967)

$$\int_0^\infty \frac{\partial^\beta f(t_D)}{\partial t_D^\beta} e^{-st_D} dt_D = s^\beta \bar{f}(s) - s^{\beta-1} f(0). \tag{48}$$

Employing the Laplace transform of Eqs. (37)–(44), one can derive the solution of the point source model (see Appendix A):

$$\bar{\psi}_{1fD} = \frac{1}{s^{1-\beta_1}} \bar{q}_D(r_D = 0, s) [FI_0(\xi_1 r_D) + K_0(\xi_1 r_D)], \tag{49}$$

where

$$F = \frac{s^{\beta_2 - \beta_1} M_{12} \xi_1 K_1(\xi_1 r_{fD}) K_0(\xi_2 r_{fD}) - g_{12} \xi_2 K_0(\xi_1 r_{fD}) K_1(\xi_2 r_{fD})}{s^{\beta_2 - \beta_1} M_{12} \xi_1 I_1(\xi_1 r_{fD}) K_0(\xi_2 r_{fD}) + g_{12} \xi_2 I_0(\xi_1 r_{fD}) K_1(\xi_2 r_{fD})}, \tag{50}$$

$$\xi_1 = \sqrt{s^{\beta_1} f_1(s)}, \tag{51}$$

$$\xi_2 = \sqrt{\frac{s^{\beta_2}}{g_{12}} f_2(s)}, \tag{52}$$

$$f_1(s) = \frac{\lambda_1 + s \omega_{1f} (1 - \omega_{1f})}{\lambda_1 + s (1 - \omega_{1f})}, \tag{53}$$

$$f_2(s) = \frac{\lambda_2 + s \omega_{2f} (1 - \omega_{2f}) \eta_{12}}{\lambda_2 + s (1 - \omega_{2f}) \eta_{12}} \eta_{12}, \tag{54}$$

$$\eta_{12} = \frac{M_{12}}{W_{12}}. \tag{55}$$

Model of the MSFH well with SRV

The pseudo-pressure solution of the point source model in a dual-porosity composite system has been derived above, and thus the pseudo-pressure solution for the MSFH well with SRV can be obtained by the superposition principle (Ozkan 1988):

$$\bar{\psi}_{1fD}(x_D, y_D, s) = \frac{1}{s^{1-\beta_1}} \sum_{i=1}^m \int_{-L_{fDi}}^{L_{fDi}} \bar{q}_{fDi}(\gamma, y_{wDi}, s) [FI_0(\xi_1 R_D) + K_0(\xi_1 R_D)] d\gamma, \tag{56}$$

where

$$R_D(x_D, y_D; \gamma) = \sqrt{(x_D - \gamma)^2 + (y_D - y_{wDi})^2}. \tag{57}$$

Based on the assumption of the infinite-conductivity hydraulic fractures, one can obtain that

$$\bar{\psi}_{wD}(s) = \bar{q}_{1fD}(x_D, y_{wDi}, s), \tag{58}$$

where $-L_{fLDi} \leq x_D \leq L_{fRDi}$.

The constraint condition of the flow rate can be expressed as

$$\sum_{i=1}^m \int_{-L_{fLDi}}^{L_{fRDi}} \bar{q}_{fD}(\gamma, y_{wDi}, s) d\gamma = \frac{1}{s}. \tag{59}$$

The model of the MSFH well with SRV including Eqs. (56)–(59) can be employed to study the pseudo-pressure behavior. The numerical discrete method (Wan 1999) will be used to solve the seepage model. The fracture wings are discretized into some segments and the flow rate in each segment is considered to stay the same at a certain time. The discrete schematic of the MSFH well in the given coordinate system is shown in Fig. 2.

And then, the discrete forms of Eqs. (56), (58) and (59) can be obtained as follows:

$$\bar{\psi}_{wD}(s) = \sum_{i=1}^m \sum_{j=1}^{2N_i} [\bar{\psi}_{1fDi,j}(x_{mDk,v}, y_{mDk,v}, s)], \tag{60}$$

$$(1 \leq v \leq 2N_k, 1 \leq k \leq m),$$

$$\sum_{i=1}^m \left\{ \sum_{j=1}^{N_i} [\bar{q}_{fDi,j}(s) \Delta L_{fLDi}] + \sum_{j=N_i+1}^{2N_i} [\bar{q}_{fDi,j}(s) \Delta L_{fRDi}] \right\} = \frac{1}{s}, \tag{61}$$

where

$$\bar{\psi}_{1fDi,j}(x_{mDk,v}, y_{mDk,v}, s) = \frac{1}{s^{1-\beta_1}} \bar{q}_{fDi,j}(s) \int_{x_{Di,j}}^{x_{Di,j+1}} [FI_0(\xi_1 R_D) + K_0(\xi_1 R_D)] d\gamma, \tag{62}$$

$$R_D(x_{mDk,v}, y_{mDk,v}; \gamma) = \sqrt{(x_{mDk,v} - \gamma)^2 + (y_{mDk,v} - y_{wDi})^2}. \tag{63}$$

Equations (60)–(63) compose $(2 \sum_{i=1}^m N_i + 1)$ linear equations with $(2 \sum_{i=1}^m N_i + 1)$ unknowns. The unknowns are $\bar{\psi}_{wD}(s)$ and $\bar{q}_{fDk,v}(s) (1 \leq v \leq 2N_k, 1 \leq k \leq m)$ which can be obtained by solving the linear equations. Finally, with the aid of the numerical inversion method (Stehfest 1970), one can obtain the bottomhole pseudo-pressure of the MSFH well with constant production rate.

Furthermore, if an MSFH well produces at a constant bottomhole pressure, the production rate of the MSFH well can be obtained by the following expression (Van Everdingen and Hurst 1949)

$$\bar{Q}_D = \frac{1}{s^2 \bar{\psi}_{wD}}. \tag{64}$$

Employing the numerical inversion method (Stehfest 1970), the production rate \bar{Q}_D in Laplace space can be transformed into the production rate Q_D in real space.

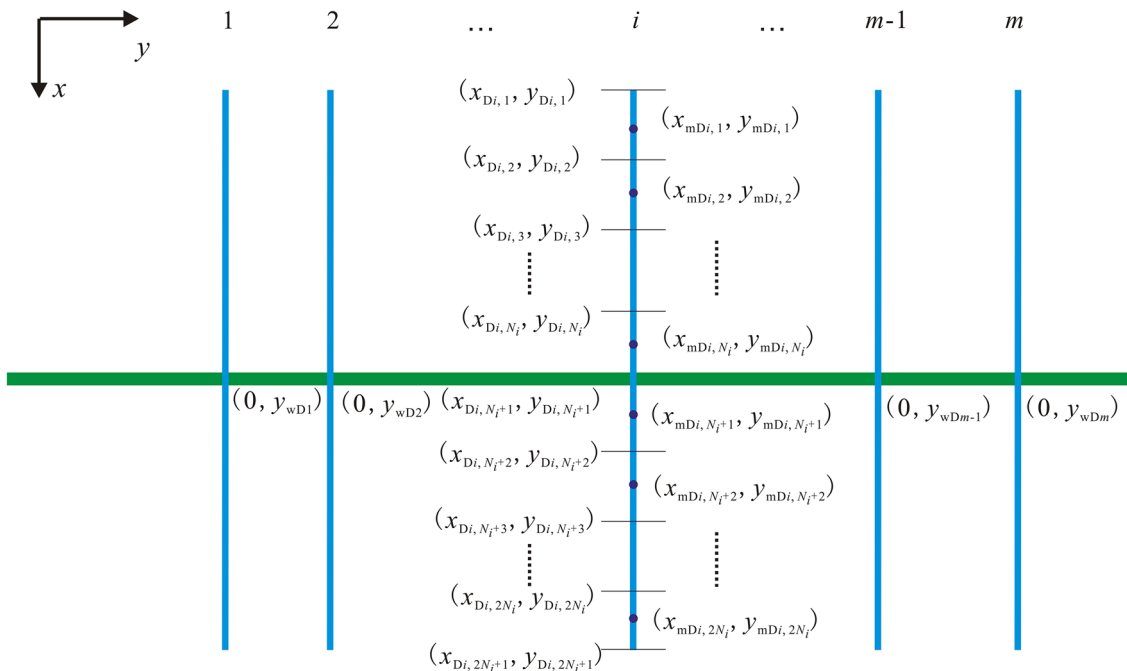


Fig. 2 Discrete schematic of the hydraulic fracture wings of an MSFH well

Results and analysis

The transient pseudo-pressure and transient rate of the MSFH well with SRV are generated based on the above model and the synthetic data listed in Table 2. The characteristics of the pseudo-pressure behavior and production rate decline are analyzed. In particular, the effects of the anomalous diffusion on the pseudo-pressure and production rate are discussed in detail.

Type curves and flow regimes

Type curves for the bottomhole pseudo-pressure of an MSFH well with SRV under the constant-rate-production (CRP) condition are shown in Fig. 3a. The type curves for the bottomhole pseudo-pressure consist of the pseudo-pressure curve (x -axis: t , y -axis: $\Delta\psi_w$) and pseudo-pressure derivative curve (x -axis: t , y -axis: $\Delta\psi_w' \cdot t$). Type curves for the production rate of an MSFH well with SRV under constant-pressure-production (CPP) condition are shown in Fig. 3b. The type curves for the production rate include the production-rate curve (x -axis: t , y -axis: Q_{sc}) and production-rate derivative curve (x -axis: t , y -axis: $-Q_{sc}' \cdot t$). Both the anomalous diffusion exponents for the SRV and URV regions are set to be 0.95. It is observed from Fig. 3

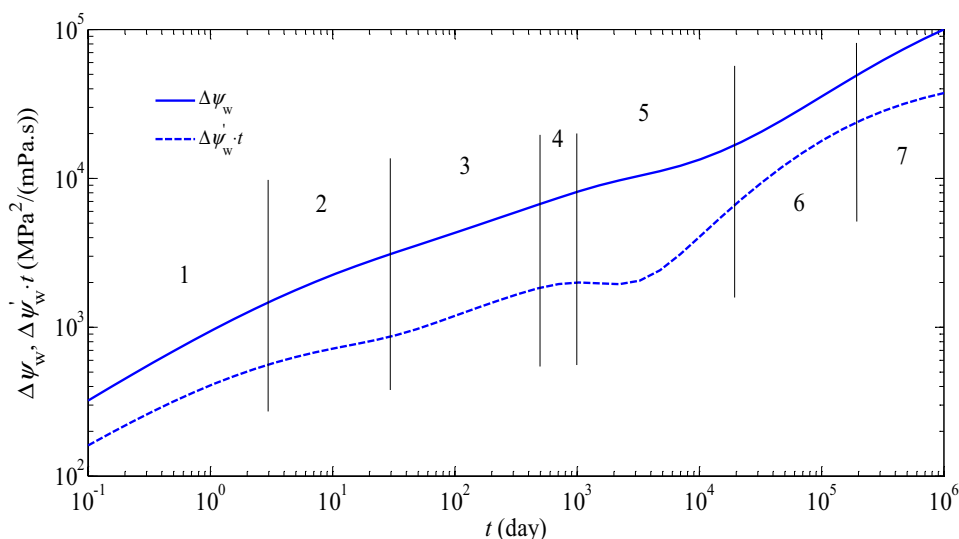
that there are seven possible flow regions in the type curves which are analyzed as follows:

1. *Early linear flow period in SRV* The linear flow appears in the area around the hydraulic fractures and is perpendicular to the lateral surface of the main hydraulic fracture. Both the pseudo-pressure derivative curve and production-rate derivative curve exhibit as straight lines. It should be noted that the slope of the pseudo-pressure derivative curve is usually greater than 0.5 due to the effect of the anomalous diffusion.
2. *Early pseudo-radial flow period in SRV* If the hydraulic-fracture spacing is relatively large, the linear flow will develop into the pseudo-radial flow before the hydraulic-fracture interference occurs. Because of the impact of the anomalous diffusion, the pseudo-pressure derivative does not keep a constant value, but increases linearly with the time.
3. *Late linear flow period in SRV* The hydraulic-fracture interference has taken place and the linear flow appears beyond the hydraulic-fracture tips. The pseudo-pressure derivative curve exhibits as a straight line, but the slope of the straight line may not be equal to 0.5 owing to the effect of the anomalous diffusion.
4. *Late pseudo-radial flow period in SRV* If the SRV radius is large enough, this flow period may be observed in

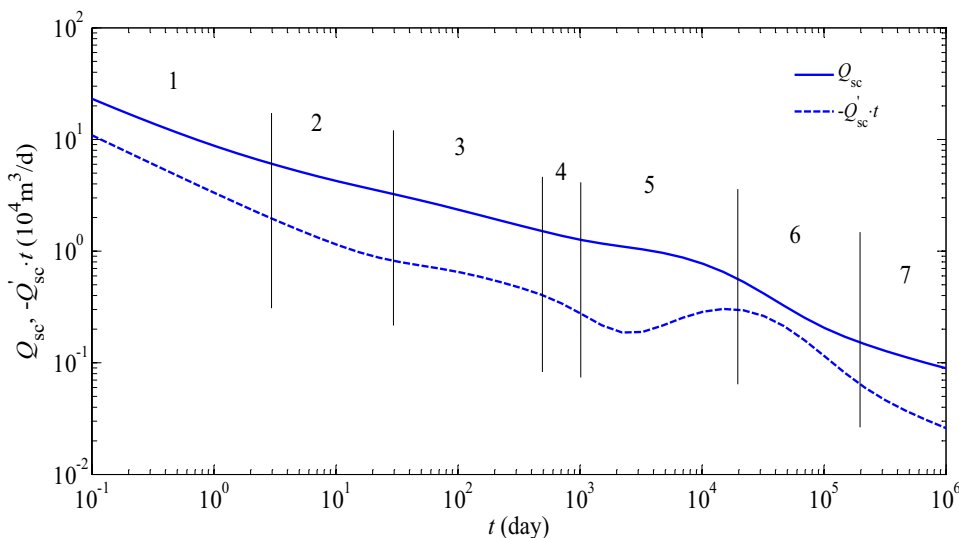
Table 2 Synthetic data used for generating type curves

Name	Value
Reservoir thickness, h , m	80
Half-length of horizontal well, L , m	400
Fracture-wing length, L_f , m	40
Hydraulic-fracture number, m	3
SRV radius, r_f , m	800
Initial reservoir pressure, p_i , MPa	60
Reservoir temperature, T , K	353
Permeability of fracture system in SRV, $k_{1\beta}$, mD/s $^{\beta_1-1}$	0.01
Permeability of matrix system in SRV, k_{1m} , mD	0.0002
Permeability of fracture system in URV, $k_{2\beta}$, mD/s $^{\beta_2-1}$	0.001
Permeability of matrix system in URV, k_{2m} , mD	0.0002
Porosity of fracture system in SRV, ϕ_{1f}	0.002
Porosity of matrix system in SRV, ϕ_{1m}	0.02
Porosity of fracture system in URV, ϕ_{2f}	0.0005
Porosity of matrix system in URV, ϕ_{2m}	0.02
Total compressibility of fracture system in SRV, c_{11f} , MPa $^{-1}$	0.028
Total compressibility of matrix system in SRV, c_{11m} , MPa $^{-1}$	0.02
Total compressibility of fracture system in URV, c_{12f} , MPa $^{-1}$	0.028
Total compressibility of matrix system in URV, c_{12m} , MPa $^{-1}$	0.02
Shape factor of SRV region, α_1 , m $^{-2}$	8×10^{-5}
Shape factor of URV region, α_2 , m $^{-2}$	8×10^{-5}
Bottomhole pressure under constant-pressure-production condition, p_w , MPa	50
Production rate under constant-rate-production condition, Q_{sc} , 10^4 m 3 /d	0.4

Fig. 3 Type curves for the bottomhole pseudo-pressure and the production rate ($\beta_1 = 0.95$, $\beta_2 = 0.95$)



(a) Type curves for the bottomhole pseudo-pressure under the CRP condition.



(b) Type curves for the production rate under the CPP condition.

type curves. The pseudo-pressure derivative curve for the pseudo-radial flow usually exhibits as a straight line. Compared with the previous flow period (i.e., late linear flow period in SRV), the slope of the pseudo-pressure derivative curve is much smaller. But in reality this flow period may not exist because of the finite area of the SRV.

5. *Matrix-fracture interporosity flow period* During this period, the interporosity flow between the matrix and fracture systems occurs, so the pseudo-pressure under the CRP condition and the production rate under the CPP condition drop more slowly compared with the previous flow periods. In this flow period, both the pseudo-

pressure derivative curve and the production-rate derivative curve exhibit as 'dip'.

6. *Transition flow period between SRV and URV* During this period, the pressure wave propagates from the SRV region to the URV region. Since the flow capability in URV is much lower than that in SRV, the pseudo-pressure drop increases rapidly under the CRP condition and the production rate decreases sharply under the CPP condition in this period. Furthermore, this period and the matrix-fracture interporosity flow period usually occur simultaneously, so type curves in this period are usually influenced by the matrix–fracture interporosity flow.

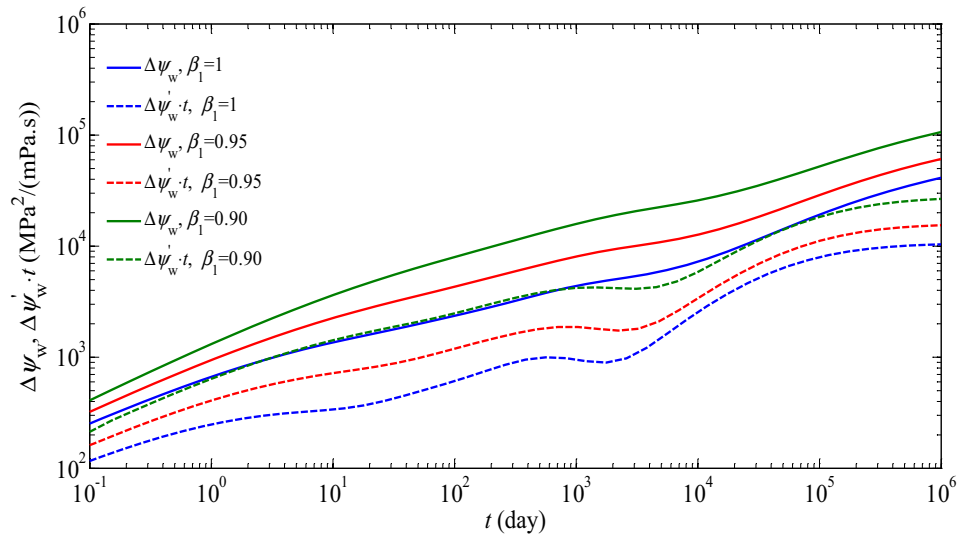
7. *Pseudo-radial flow period in URV* When the pressure wave continues to travel in the URV region, the transition flow will develop into the pseudo-radial flow. In this period, slower growth of the pseudo-pressure drop under the CRP condition is observed and the production rate under the CPP condition decreases more slowly. Similarly, the magnitude of the pseudo-pressure derivative in this flow regime increases linearly with the time because of the effect of the anomalous diffusion.

Sensitivity analysis

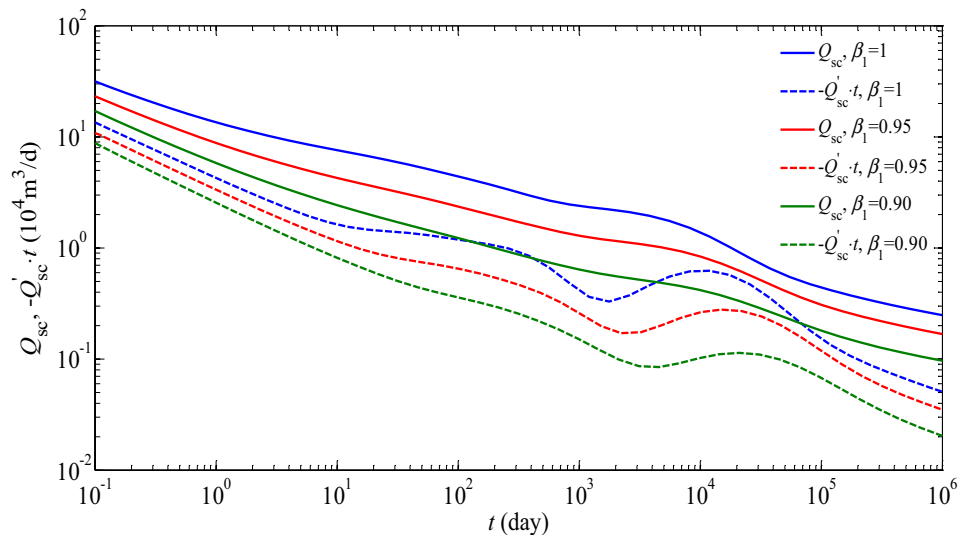
Figure 4 shows the bottomhole pseudo-pressure under the CRP condition and the production rate under the CPP condition with different values of anomalous diffusion exponent

in SRV region (β_1). It is obvious that β_1 has important effects on the pseudo-pressure behavior and production-rate performance in all flow periods. As the magnitude of the β_1 decreases, the pseudo-pressure drop becomes larger under the CRP condition and the production rate gets smaller under the CPP condition. Hence, the existence of the anomalous diffusion has a negative impact on the production performance of the MSFH well. The smaller the value of the β_1 is, the worse the production performance of the MSFH well is. Furthermore, with decreasing the value of the β_1 , the duration of the linear flow becomes longer and the slopes of the pseudo-pressure derivative curves in the linear flow period and pseudo-radial flow period increase. It is interesting that the ‘dip’ in the pseudo-pressure derivative curve and the

Fig. 4 Effects of β_1 on the bottomhole pseudo-pressure and the production rate ($\beta_2 = 1$)



(a) Effect of β_1 on the bottomhole pseudo-pressure under the CRP condition.



(b) Effect of β_1 on the production rate under the CPP condition.

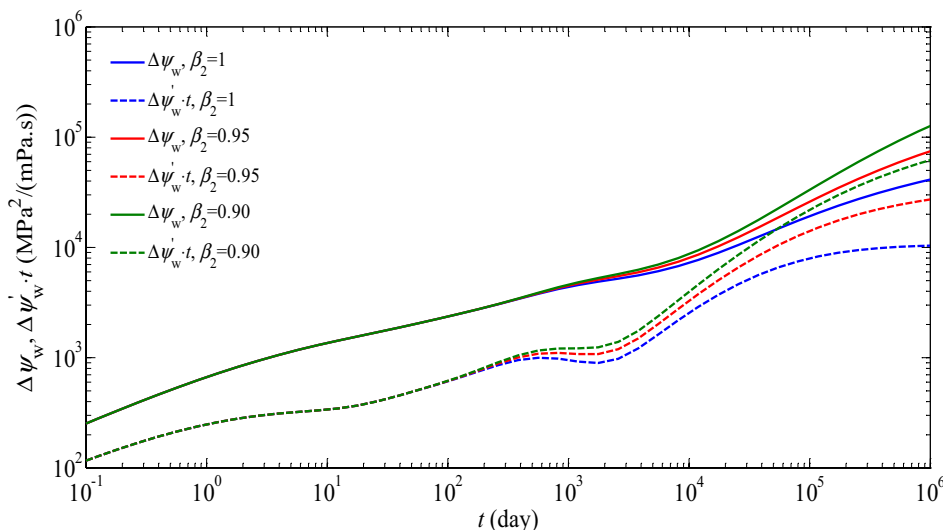
production-rate derivative curve is shifted right and becomes shallower when the β_1 decreases.

Figure 5 shows the bottomhole pseudo-pressure under the CRP condition and the production rate under the CPP condition with different values of anomalous diffusion exponent in URV region (β_2). It can be observed that the β_2 only has an effect on the transient flow after the pressure wave propagates outside the SRV region. Decreasing the value of the β_2 gives rise to the increase of the pseudo-pressure drop in the CRP case and the decrease of the production rate in the CPP case. Furthermore, as the magnitude of the β_2 decreases, the ‘dip’ in the pseudo-pressure derivative curve and the production-rate derivative curve becomes shallower, indicating that the influence of the matrix-fracture interporosity flow on the performance of the MSFH well has been reduced.

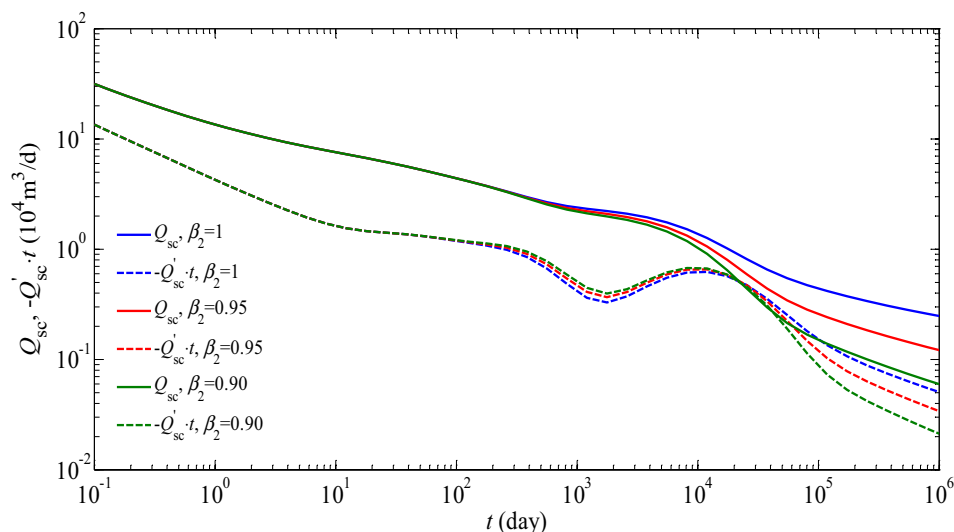
When $\beta_2 < 1$, the slope of the pseudo-pressure derivative curve in the pseudo-radial flow period is greater than zero and increases with the decrease of the β_2 .

Figure 6 shows the comparisons between the effects of β_1 and β_2 on the bottomhole pseudo-pressure under the CRP condition and the production rate under the CPP condition. It is interesting to find that both the β_1 and β_2 have effects on the pseudo-pressure behavior and production-rate performance in the flow periods after the pressure wave propagates outside the SRV region, but the effect of the β_2 is more pronounced than that of the β_1 in these flow periods. Therefore, it is concluded that the β_1 has a main effect on the production performance of the MSFH well in early flow periods, and the effect of the β_2 becomes more important than that of the β_1 in late flow periods.

Fig. 5 Effects of β_2 on the bottomhole pseudo-pressure and the production rate ($\beta_1 = 1$)

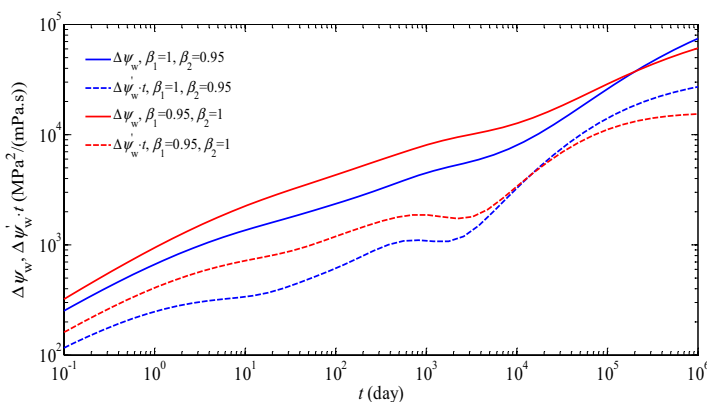


(a) Effect of β_2 on the bottomhole pseudo-pressure under the CRP condition.

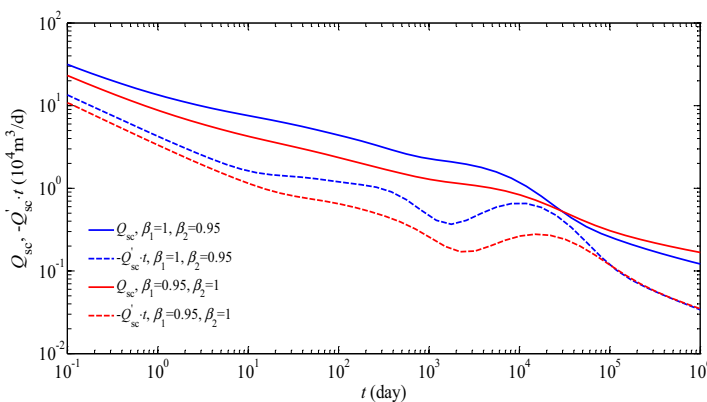


(b) Effect of β_2 on the production rate under the CPP condition.

Fig. 6 Comparisons between the effects of β_1 and β_2 on the bottomhole pseudo-pressure and the production rate



(a) Comparison between the effects of β_1 and β_2 on the bottomhole pseudo-pressure under the CRP condition.



(b) Comparison between the effects of β_1 and β_2 on the production rate under the CPP condition.

Figure 7 shows the bottomhole pseudo-pressure under the CRP condition and the production rate under the CPP condition with different values of the permeability of fracture system in SRV ($k_{1\beta}$). It is seen that the $k_{1\beta}$ affects the pseudo-pressure behavior and production-rate performance in the entire flow periods: A significant influence of the $k_{1\beta}$ on type curves is shown before the pressure wave propagates outside the SRV, while the influence of the $k_{1\beta}$ on type curves decreases with the increase of the time after the pressure wave propagates outside the SRV. Increasing the $k_{1\beta}$ reduces the pseudo-pressure drop in the CRP case and enhances the production rate in the CPP case. Therefore, improving the permeability of the SRV region is critical to obtain good performance of the MSFH well. Furthermore, as the magnitude of the $k_{1\beta}$ increases, the duration of the early linear flow period in SRV is shorter and the transition flow period between the SRV and URV regions appears earlier.

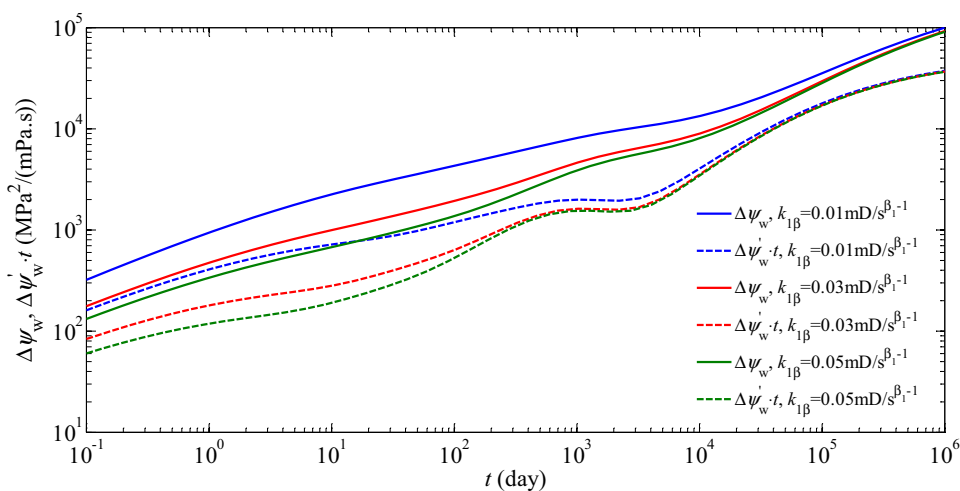
Figure 8 shows the bottomhole pseudo-pressure under the CRP condition and the production rate under the CPP condition with different values of the permeability of fracture

system in URV ($k_{2\beta}$). It is clear that the $k_{2\beta}$ has no effect on the pseudo-pressure behavior and production-rate performance before the pressure wave arrives at the interface between the SRV and URV regions. After the pressure wave goes into the URV region, smaller value of $k_{2\beta}$ results in a substantial increase of the pseudo-pressure drop under the CRP condition and a large decrease of the production rate under the CPP condition. Therefore, compared with the $k_{1\beta}$, the $k_{2\beta}$ has a more significant effect on the performance of the MSFH well in the late flow periods.

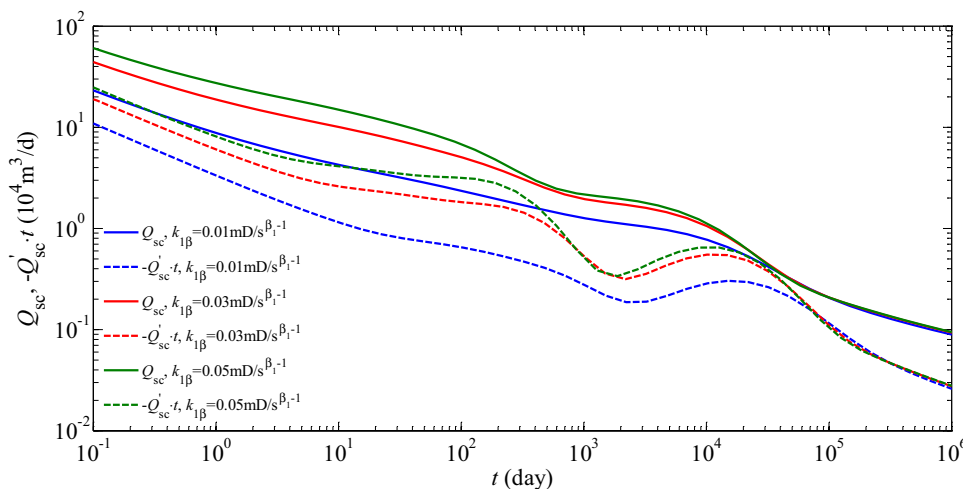
Conclusions

We have incorporated the fractional Darcy law into the governing equations and established a novel model for the MSFH well with SRV. The proposed model includes anomalous diffusion exponents for the SRV region and the URV region, respectively, and thus this model has a much wider field of

Fig. 7 Effect of $k_{1\beta}$ on the bottomhole pseudo-pressure and the production rate ($\beta_1 = 0.95$, $\beta_2 = 0.95$)



(a) Effect of $k_{1\beta}$ on the bottomhole pseudo-pressure under the CRP condition.

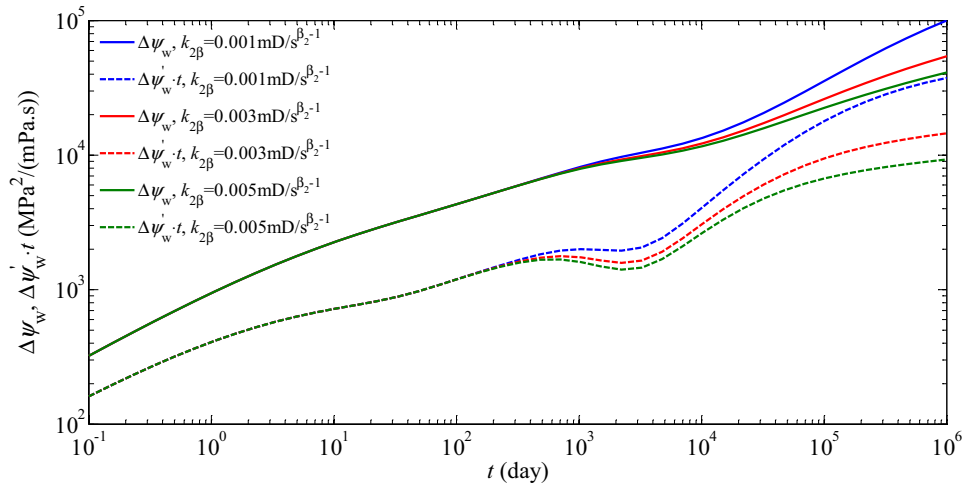


(b) Effect of $k_{1\beta}$ on the production rate under the CPP condition.

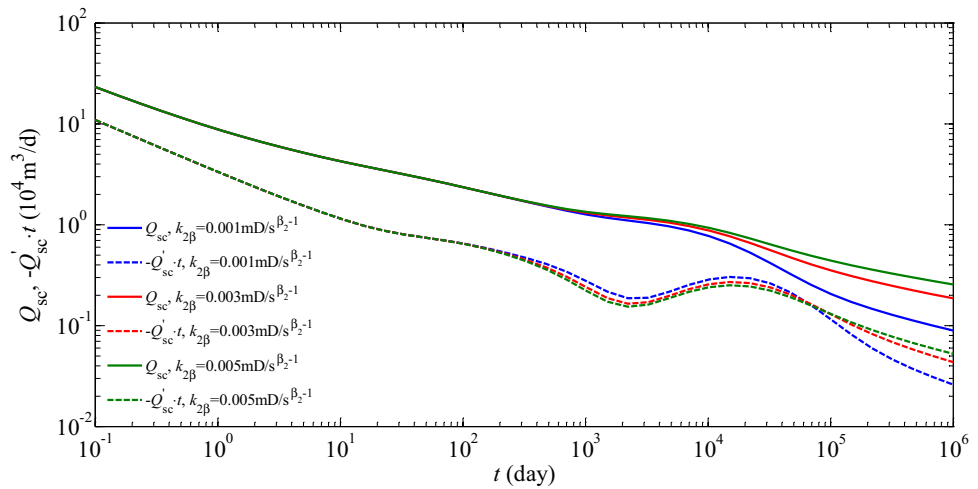
application and is more suitable for fractured reservoirs compared to the conventional models. The semi-analytical solution of the fractional model is derived, and type curves for pseudo-pressure and production rate are plotted. The influence of the relevant parameters on pseudo-pressure behavior and production rate decline is analyzed in detail. It is found that anomalous diffusion exponent has significant effects on the characteristics of the pseudo-pressure behavior and production rate decline. As the magnitude of anomalous diffusion exponent

decreases, the pseudo-pressure drop becomes larger under the CRP condition and the production rate becomes smaller under the CPP condition. Furthermore, the anomalous diffusion has an effect on the characteristic of the type curves in different flow periods. The proposed model extends the conventional model of the MSFH well with SRV to take into account the effect of the anomalous diffusion, and thus it has an advantage over the previous models in interpreting production data and forecasting production performance.

Fig. 8 Effect of $k_{2\beta}$ on the bottomhole pseudo-pressure and the production rate ($\beta_1 = 0.95$, $\beta_2 = 0.95$)



(a) Effect of $k_{2\beta}$ on the bottomhole pseudo-pressure under the CRP condition.



(b) Effect of $k_{2\beta}$ on the production rate under the CPP condition.

Acknowledgements We acknowledge the support provided by Open Fund of State Key Laboratory of Oil and Gas Reservoir Geology and Exploitation (PLN201627), the Scientific Research Starting Project of SWPU (2017QHZ031), the Natural Science Project of Sichuan Province Department of Education (17ZA0425), Young Scholars Development Fund of SWPU (201599010100).

Appendix A

Employing the Laplace transform of Eqs. (37)–(44) yields that

$$s^{1-\beta_1} \left[\frac{1}{r_D} \frac{\partial}{\partial r_D} \left(r_D \frac{\partial \bar{\psi}_{1FD}}{\partial r_D} \right) \right] = \omega_{1f} s \bar{\psi}_{1FD} + \lambda_1 (\bar{\psi}_{1FD} - \bar{\psi}_{1mD}), \quad (65)$$

$(0 \leq r_D \leq r_{fD}),$

$$(1 - \omega_{1f}) s \bar{\psi}_{1mD} - \lambda_1 (\bar{\psi}_{1FD} - \bar{\psi}_{1mD}) = 0, \quad (0 \leq r_D \leq r_{fD}), \quad (66)$$

$$s^{1-\beta_2} \left[\frac{g_{12}}{r_D} \frac{\partial}{\partial r_D} \left(r_D \frac{\partial \bar{\psi}_{2FD}}{\partial r_D} \right) \right] = \frac{M_{12} \omega_{2f}}{W_{12}} s \bar{\psi}_{2FD} + \lambda_2 (\bar{\psi}_{2FD} - \bar{\psi}_{2mD}), \quad (r_{fD} \leq r_D < \infty), \quad (67)$$

$$\frac{M_{12} (1 - \omega_{2f})}{W_{12}} s \bar{\psi}_{2mD} - \lambda_2 (\bar{\psi}_{2FD} - \bar{\psi}_{2mD}) = 0, \quad (r_{fD} \leq r_D < \infty), \quad (68)$$

$$\lim_{r_D \rightarrow 0} \left(r_D \frac{\partial \bar{\psi}_{1FD}}{\partial r_D} \right) = -\frac{1}{s^{1-\beta_1}} \bar{q}_D (r_D = 0, s), \quad (69)$$

$$\bar{\psi}_{2FD} (r_D \rightarrow \infty, s) = 0, \quad (70)$$

$$\bar{\psi}_{1FD} (r_D = r_{fD}, s) = \bar{\psi}_{2FD} (r_D = r_{fD}, s), \quad (71)$$

$$\left. \frac{\partial \bar{\psi}_{1FD}}{\partial r_D} \right|_{r_D=r_{fD}} = \frac{g_{12}}{M_{12} s^{\beta_2-\beta_1}} \left. \frac{\partial \bar{\psi}_{2FD}}{\partial r_D} \right|_{r_D=r_{fD}}. \quad (72)$$

Combining Eq. (66) with Eq. (65) yields that

$$\frac{\partial^2 \bar{\psi}_{1fD}}{\partial r_D^2} + \frac{1}{r_D} \frac{\partial \bar{\psi}_{1fD}}{\partial r_D} = s^{\beta_1} f_1(s) \bar{\psi}_{1fD}, \quad (0 \leq r_D \leq r_{fD}), \quad (73)$$

where

$$f_1(s) = \frac{\lambda_1 + s\omega_{1f}(1 - \omega_{1f})}{\lambda_1 + s(1 - \omega_{1f})}. \quad (74)$$

Similarly, according to Eqs. (67) and (68), one can obtain that

$$\frac{\partial^2 \bar{\psi}_{2fD}}{\partial r_D^2} + \frac{1}{r_D} \frac{\partial \bar{\psi}_{2fD}}{\partial r_D} = \frac{s^{\beta_2}}{g_{12}} f_2(s) \bar{\psi}_{2fD}, \quad (r_{fD} \leq r_D < \infty), \quad (75)$$

where

$$f_2(s) = \frac{\lambda_2 + s\omega_{2f}(1 - \omega_{2f})\eta_{12}}{\lambda_2 + s(1 - \omega_{2f})\eta_{12}}, \quad (76)$$

$$\eta_{12} = \frac{M_{12}}{W_{12}}. \quad (77)$$

The general solutions of Eqs. (73) and (75) are

$$\bar{\psi}_{1fD} = A_1 I_0 \left(\sqrt{s^{\beta_1} f_1(s) r_D} \right) + B_1 K_0 \left(\sqrt{s^{\beta_1} f_1(s) r_D} \right), \quad (78)$$

$$\bar{\psi}_{2fD} = A_2 I_0 \left(\sqrt{\frac{s^{\beta_2}}{g_{12}} f_2(s) r_D} \right) + B_2 K_0 \left(\sqrt{\frac{s^{\beta_2}}{g_{12}} f_2(s) r_D} \right). \quad (79)$$

With the aid of Eq. (70), one can obtain that

$$A_2 = 0. \quad (80)$$

Taking Eq. (78) into Eq. (69), one can obtain that

$$B_1 = \frac{1}{s^{1-\beta_1}} \bar{q}_D(r_D = 0, s). \quad (81)$$

Substituting Eqs. (78) and (79) into Eqs. (71) and (72), one can derive that

$$A_1 I_0(\xi_1 r_{fD}) + B_1 K_0(\xi_1 r_{fD}) = B_2 K_0(\xi_2 r_{fD}), \quad (82)$$

$$A_1 I_1(\xi_1 r_{fD}) - B_1 K_1(\xi_1 r_{fD}) = -B_2 \frac{g_{12} \xi_2}{s^{\beta_2 - \beta_1} M_{12} \xi_1} K_1(\xi_2 r_{fD}), \quad (83)$$

where

$$\xi_1 = \sqrt{s^{\beta_1} f_1(s)}, \quad (84)$$

$$\xi_2 = \sqrt{\frac{s^{\beta_2}}{g_{12}} f_2(s)}. \quad (85)$$

Combining Eq. (82) with Eq. (83), one can obtain the relationship between A_1 and B_1 as follows:

$$A_1 = B_1 \frac{s^{\beta_2 - \beta_1} M_{12} \xi_1 K_1(\xi_1 r_{fD}) K_0(\xi_2 r_{fD}) - g_{12} \xi_2 K_0(\xi_1 r_{fD}) K_1(\xi_2 r_{fD})}{s^{\beta_2 - \beta_1} M_{12} \xi_1 I_1(\xi_1 r_{fD}) K_0(\xi_2 r_{fD}) + g_{12} \xi_2 I_0(\xi_1 r_{fD}) K_1(\xi_2 r_{fD})}. \quad (86)$$

Substituting Eqs. (81) and (86) into Eq. (78) yields that

$$\bar{\psi}_{1fD} = \frac{1}{s^{1-\beta_1}} \bar{q}_D(r_D = 0, s) [F I_0(\xi_1 r_D) + K_0(\xi_1 r_D)], \quad (87)$$

where

$$F = \frac{s^{\beta_2 - \beta_1} M_{12} \xi_1 K_1(\xi_1 r_{fD}) K_0(\xi_2 r_{fD}) - g_{12} \xi_2 K_0(\xi_1 r_{fD}) K_1(\xi_2 r_{fD})}{s^{\beta_2 - \beta_1} M_{12} \xi_1 I_1(\xi_1 r_{fD}) K_0(\xi_2 r_{fD}) + g_{12} \xi_2 I_0(\xi_1 r_{fD}) K_1(\xi_2 r_{fD})}. \quad (88)$$

References

Apaydin OG, Ozkan E, Raghavan R (2012) Effect of discontinuous microfractures on ultratight matrix permeability of a dual-porosity medium. *SPE Reserv Eval Eng* 15(4):473–485

Caputo M (1967) Linear models of dissipation whose Q is almost frequency independent-II. *Geophys J R Astron Soc* 13(5):529–539

Chen P, Jiang S, Chen Y, Zhang K (2018) Pressure response and production performance of volumetric fracturing horizontal well in shale gas reservoir based on boundary element method. *Eng Anal Bound Elem* 87:66–77

Clarkson CR (2013) Production data analysis of unconventional gas wells: review of theory and best practices. *Int J Coal Geol* 109–110:101–146

Feng Q, Meng F (2017) Traveling wave solutions for fractional partial differential equations arising in mathematical physics by an improved fractional Jacobi elliptic equation method. *Math Method Appl Sci* 40(10):3676–3686

Guo Y (2010) Nontrivial solutions for boundary-value problems of nonlinear fractional differential equations. *Bull Korean Math Soc* 47(1):81–87

Guo J, Wang H, Zhang L (2016) Transient pressure and production dynamics of multi-stage fractured horizontal wells in shale gas reservoirs with stimulated reservoir volume. *J Nat Gas Sci Eng* 35:425–443

Hao X, Wang H, Liu L, Cui Y (2017) Positive solutions for a system of nonlinear fractional nonlocal boundary value problems with parameters and p-Laplacian operator. *Bound Value Probl* 2017(1):182

Jiang J, Liu L, Wu Y (2013) Positive solutions to singular fractional differential system with coupled boundary conditions. *Commun Nonlinear Sci Numer Simulat* 18(11):3061–3074

Li M, Wang J (2018) Exploring delayed Mittag-Leffler type matrix functions to study finite time stability of fractional delay differential equations. *Appl Math Comput* 324:254–265

Mayerhofer MJ, Lolon E, Warpinski NR, Cipolla CL, Walser DW, Rightmire CM (2010) What is stimulated reservoir volume? *SPE Prod Oper* 25(1):89–98

Obembe AD, Al-Yousef HY, Hossain ME, Abu-Khamsin SA (2017) Fractional derivatives and their applications in reservoir engineering problems: a review. *J Pet Sci Eng* 157:312–327

- Ozkan E (1988) Performance of horizontal wells. Dissertation, University of Tulsa
- Ozkan E, Brown ML, Raghavan R, Kazemi H (2011) Comparison of fractured-horizontal-well performance in tight sand and shale reservoirs. *SPE Reserv Eval Eng* 14(2):248–259
- Raghavan R (2012a) Fractional derivatives: application to transient flow. *J Pet Sci Eng* 80:7–13
- Raghavan R (2012b) Fractional diffusion: performance of fractured wells. *J Pet Sci Eng* 92–93:167–173
- Raghavan R, Chen C (2013a) Fractured-well performance under anomalous diffusion. *SPE Reser Eval Eng* 16(3):237–245
- Raghavan R, Chen C (2013b) Fractional diffusion in rocks produced by horizontal wells with multiple, transverse hydraulic fractures of finite conductivity. *J Pet Sci Eng* 109:133–143
- Raghavan R, Chen C (2015) Anomalous subdiffusion to a horizontal well by a subordinator. *Transp Porous Med* 107(2):387–401
- Raghavan R, Chen C (2017) Addressing the influence of a heterogeneous matrix on well performance in fractured rocks. *Transp Porous Med* 117(1):69–102
- Razminia K, Razminia A, Tenreiro Machado JA (2014) Analysis of diffusion process in fractured reservoirs using fractional derivative approach. *Commun Nonlinear Sci Numer Simulat* 19:3161–3170
- Ren J, Guo P (2015) Anomalous diffusion performance of multiple fractured horizontal wells in shale gas reservoirs. *J Nat Gas Sci Eng* 26:642–651
- Ren J, Guo P (2017) Nonlinear flow model of multiple fractured horizontal wells with stimulated reservoir volume including the quadratic gradient term. *J Hydrol* 554:155–172
- Ren J, Guo P (2018a) Nonlinear seepage model for multiple fractured horizontal wells with the effect of the quadratic gradient term. *J Porous Media* 21(3):223–239
- Ren J, Guo P (2018b) A general analytical method for transient flow rate with the stress-sensitive effect. *J Hydrol* 565:262–275
- Ren J, Guo P (2018c) Analytical method for transient flow rate with the effect of the quadratic gradient term. *J Pet Sci Eng* 162:774–784
- Shen T, Xin J, Huang J (2018) Time-space fractional stochastic Ginzburg-Landau equation driven by Gaussian white noise. *Stoch Anal Appl* 36(1):103–113
- Stalgorova E, Mattar L (2012) Analytical model for history matching and forecasting production in multfrac composite systems. In: SPE Paper 162516 presented at SPE Canadian Unconventional Resources Conference, Calgary, Alberta
- Stehfest H (1970) Numerical inversion of Laplace transforms. *Commun ACM* 13:47–49
- Tian L, Xiao C, Liu M, Gu D, Song G, Cao H, Li X (2014) Well testing model for multi-fractured horizontal well for shale gas reservoirs with consideration of dual diffusion in matrix. *J Nat Gas Sci Eng* 21:283–295
- Van Everdingen AF, Hurst W (1949) The application of the Laplace transformation to flow problems in reservoirs. *Trans AIME* 186:305–324
- Wan J (1999) Well models of hydraulically fractured horizontal wells. Dissertation, Stanford University
- Wang Y, Yi X (2017) Transient pressure behavior of a fractured vertical well with a finite-conductivity fracture in triple media carbonate reservoir. *J Porous Media* 20(8):707–722
- Wang Y, Yi X (2018) Flow modeling of well test analysis for a multiple-fractured horizontal well in triple media carbonate reservoir. *Int J Nonlinear Sci Numer Simul* 19(5):439–457
- Wang Y, Tao Z, Chen L, Ma X (2017) The nonlinear oil-water two-phase flow behavior for a horizontal well in triple media carbonate reservoir. *Acta Geophys* 65(5):977–989
- Warren JE, Root PJ (1963) The behavior of naturally fractured reservoirs. *SPE J* 3(3):245–255
- Wei M, Duan Y, Fang Q, Zhang T (2016) Production decline analysis for a multi-fractured horizontal well considering elliptical reservoir stimulated volumes in shale gas reservoirs. *J Geophys Eng* 13(3):354–365
- Xu R, Meng F (2016) Some new weakly singular integral inequalities and their applications to fractional differential equations. *J Inequal Appl* 2016(1):78
- Xu J, Guo C, Wei M, Jiang R (2015a) Production performance analysis for composite shale gas reservoir considering multiple transport mechanisms. *J Nat Gas Sci Eng* 26:382–395
- Xu J, Guo C, Teng W, Wei M, Jiang R (2015b) Production performance analysis of tight oil/gas reservoirs considering stimulated reservoir volume using elliptical flow. *J Nat Gas Sci Eng* 26:827–839
- Yuan B, Su Y, Moghanloo RG, Rui Z, Wang W, Shang Y (2015) A new analytical multi-linear solution for gas flow toward fractured horizontal wells with different fracture intensity. *J Nat Gas Sci Eng* 23:227–238
- Zeng H, Fan D, Yao J, Sun H (2015) Pressure and rate transient analysis of composite shale gas reservoirs considering multiple mechanisms. *J Nat Gas Sci Eng* 27:914–925
- Zhang K (2017) On a sign-changing solution for some fractional differential equations. *Bound Value Probl* 2017(1):59
- Zhang X, Liu L, Wu Y (2014) The uniqueness of positive solution for a fractional order model of turbulent flow in a porous medium. *Appl Math Lett* 37:26–33
- Zhang X, Liu L, Wu Y, Wiwatanapataphee B (2017) Nontrivial solutions for a fractional advection dispersion equation in anomalous diffusion. *Appl Math Lett* 66:1–8
- Zhao YL, Zhang LH, Luo JX, Zhang BN (2014) Performance of fractured horizontal well with stimulated reservoir volume in unconventional gas reservoir. *J Hydrol* 512:447–456
- Zhu B, Liu L, Wu Y (2016) Local and global existence of mild solutions for a class of nonlinear fractional reaction–diffusion equations with delay. *Appl Math Lett* 61:73–79
- Zuo M, Hao X, Liu L, Cui Y (2017) Existence results for impulsive fractional integro-differential equation of mixed type with constant coefficient and antiperiodic boundary conditions. *Bound Value Probl* 2017(1):161